CORROSION SCIENCE AND TECHNOLOGY, Vol.22, No.2(2023), pp.90~98 pISSN 1598-6462 / eISSN 2288-6524
[Research Paper] DOI: https://doi.org/10.14773/cst.2023.22.2.90

Corrosion Protection Properties of Co_3O_4 and $CoFe_2O_4$ Nanoparticles for Water-Based Epoxy Coatings on 2024-T3 Aluminum Alloys

Thu Thuy Thai[1,†], Anh Truc Trinh[1,†], Thi Thanh Tam Pham[2], and Hoan Nguyen Xuan[2]

[1]*Institute for Tropical Technology, Vietnam Academy of Science and Technology, 18 Hoang Quoc Viet, Hanoi 122000, Vietnam*
[2]*Faculty of Chemistry, VNU University of Science, Vietnam National University, 19 Le Thanh Tong, Hoan Kiem, Hanoi 110000, Vietnam*
(Received December 03, 2020; Revised March 19, 2021; Accepted March 30, 2022)

In this study, cobalt oxide (Co_3O_4) and cobalt-doped magnetite ($CoFe_2O_4$) nanoparticles were synthesized by a hydrothermal method. They were then used as corrosion inhibitors for corrosion protection of AA2024-T3 aluminum alloys. These obtained nanoparticles were characterized by x-ray diffraction, field-emission scanning electron microscopy, and Zeta potential measurements. Corrosion inhibition activities of Co_3O_4 and $CoFe_2O_4$ nanoparticles were determined by performing electrochemical measurements for bare AA2024-T3 aluminum alloys in 0.05 M NaCl + 0.1 M Na_2SO_4 solution containing Co_3O_4 or $CoFe_2O_4$ nanoparticles. Corrosion protection for AA2024-T3 aluminum alloys by a water-based epoxy with or without the synthesized Co_3O_4 or $CoFe_2O_4$ nanoparticles was investigated by electrochemical impedance spectroscopy during immersion in 0.1 M NaCl solution. The corrosion protection of epoxy coating deposited on the AA2024-T3 surface was improved by incorporating Co_3O_4 or $CoFe_2O_4$ nanoparticles in the coating. The corrosion protection performance of the epoxy coating containing $CoFe_2O_4$ was higher than that of the epoxy coating containing Co_3O_4.

Keywords: *Aluminum alloy, Cobalt oxide nanoparticle, Cobalt-doped magnetite, Corrosion inhibition, EIS*

1. Introduction

Since the beginning of the 1990s, the high toxicity associated with hexavalent chromium, used as an inhibitive pigment, has imposed restrictions on its use in industrial applications. Today, the development of new Cr-free systems remains a significant challenge.

Transition metals have been early used as inhibitors for corrosion protection of various metal substrates. Chromate pigment is the most efficient inhibitor, but the toxicity and carcinogenic effects of Cr (VI) compounds on human health are serious problems. New regulations are restricting and gradually eliminating their use now and in the future. Nickel and cobalt cations have been studied as alternative inhibitors for corrosion resistance of zinc or galvanized zinc [1,2]. X-ray photoelectron spectroscopy (XPS) and Mössbauer studies showed the formation of $Co(OH)_2$ on the zinc surface when immerging in the $CoCl_2$ solution at low concentration, which reduced the corrosion rate of the metal. Cobalt cations in solution and conversion coating were also reported as promising inhibitors for corrosion protection of aluminum alloys [3-6]. Their effectiveness is attributed to the limitation of the oxygen reduction reaction and the diffusion blockage of corrosion agents by forming of an oxide/ a hydroxide film on the aluminum surface.

Following this approach, cobalt-containing compounds could be considered inhibitive pigments in the primer for corrosion resistance of carbon steel or aluminum substrates. The electrochemical impedance spectroscopy (EIS) coupled with salt spray results exhibited a substantial improvement of the inhibitive property of ZnO nanoparticles when doped with cobalt. The cobalt action is attributed to accelerating the solubility of zinc inhibitor for enhancing the inhibitive performance beneath the coating. In the same way, Co-doped Al_2O_3 nanoparticles have been used in the epoxy coating applied on the 1050 aluminum alloy substrate. The extract solution of $CoAl_2O_4$ shows a mixed cathodic and anodic inhibition performance compared to that of Al_2O_3. This is due to the release of the Co^{2+} from $CoAl_2O_4$ nanoparticles and then forming a protective layer ($Co(OH)_2$) on the active sites of aluminum, limiting the access of corrosion species to the aluminum surface.

In the previous work [7], cobalt-doped magnetite (Co-doped magnetite) nanoparticles were prepared and incorporated into an epoxy resin for the corrosion protection of carbon steel. The presence of a low concentration of $CoFe_2O_4$ (3 wt%) in the coating significantly reinforced the protection property of the coating. The barrier property of the coating was high with the low proportion of Co-doped in the magnetite (2.5 wt%) compared with the higher content (5.0 wt% and 7.5 wt%). The improvement of film adherence was achieved with the presence of Co-doped magnetite in the coating; this was proved by the

†Corresponding author: anhtruc.trinh@itt.vast.vn, ttthuy@itt.vast.vn

interaction at the coating/steel interface of Co^{2+} cations. It was noteworthy that the improvement of the coating had a weak effect at high content of Co^{2+} in the magnetite (5.0 wt% and 7.5 wt%); this may be attributed to the high release of the Co^{2+} cations, leading to a decrease in the barrier effect of the coating.

In this study, cobalt oxide nanoparticles (Co_3O_4) were prepared by hydrothermal method and then dispersed into an epoxy resin for reinforcing the corrosion protection of the coating on the aluminum alloy surface. The protection behaviors were compared with Co-doped magnetite nanoparticles.

2. Materials and methods

2.1 Materials

2024 aluminum alloy (AA2024) was supplied by Mapaero company, France. For electrochemical measurements in the solution, a rod with a naked 1 cm^2 area surface was carefully polished with SiC paper from 80 to 1200 grade, rinsed with absolute ethanol, quickly dried, and immediately immersed in the studied solution.

The following chemical precursors were used for synthesis: $FeCl_3.6H_2O$ (>99%, Merck), $FeSO_4.7H_2O$ (>99%, Merck), $CoCl_2.6H_2O$ (> 98%, Merck), KOH (>82%, Merck), ethanol (>99.5°, Merck) and H_2O_2 (Vietnam).

The cobalt-doped magnetite nanoparticles were prepared following the protocol previously used [8] and is briefly recalled here: a mixture of $FeCl_3.6H_2O$/ $FeSO_4.7H_2O$ was dissolved in a beaker containing distilled water. After that, *m* (g) of $CoCl_2.6H_2O$ salt was added to this mixture, concerning the theoretical quantity of Co doping in magnetite particles (1.0 and 2.5 in weight percent). Under stirring, KOH solution was added into the mixture until the precipitate occurred and then transferred to Teflon-lined stainless steel, non-stirred autoclave, and sealed. The reaction was conducted for 7 hours at 150 °C. After the reaction, the products were washed with distilled water and absolute alcohol to remove impurity ions. The obtained products were dried in an oven at 80 °C for 12 hours. After that, the obtained cobalt-doped magnetite samples were denoted by Fe_3O_4.Co *x* wt% (*x* =1.0, and 2.5).

The cobalt oxide nanoparticles (Co_3O_4) were prepared following process: firstly, the $CoCl_2.6H_2O$ salt was dissolved in a beaker containing distilled water and H_2O_2 to oxidize Co(II) cations to Co(III) under a magnetic stirrer at room temperature for 30 minutes. The $CoCl_2.6H_2O$ salt was added to obtain the mixture of $CoCl_3$/ $CoCl_2$. Afterward, the KOH solution was adjusted into this mixture until the precipitate occurred, then underwent the hydrothermal treatment in the same as the previous protocol prepared of cobalt-doped magnetite nanoparticles. The procedures of synthesis are detailed in Fig. 1.

The binder was water-based epoxy resin, composing YD828 as resin and Epicure 8537 as curing agents. The epoxy coating was deposited on the AA2024 surface by Filmfuge Paint Spinner Ref 110N (Sheen, United Kingdom) equipment.

AA2024 sheets (60 × 40 × 1 mm) were used as substrates for the coating. They were cleaned with ethanol before applying the coating.

The Co oxide and Co-doped magnetite nanoparticles were incorporated into the epoxy coating at a concentration of 5 wt%. The liquid paints (pure epoxy and epoxy resin containing Co oxide or Co-doped magnetite nanoparticles) were applied by spin coating with a speed of 600 rpm for 20 s. After drying (ambient temperature for 24 h), the coatings were about 30 µm in thickness (measured by a Minitest 600 Erichsen digital meter).

2.2 Analytical characterizations

XRD patterns were recorded on D5000 Siemens diffractometer

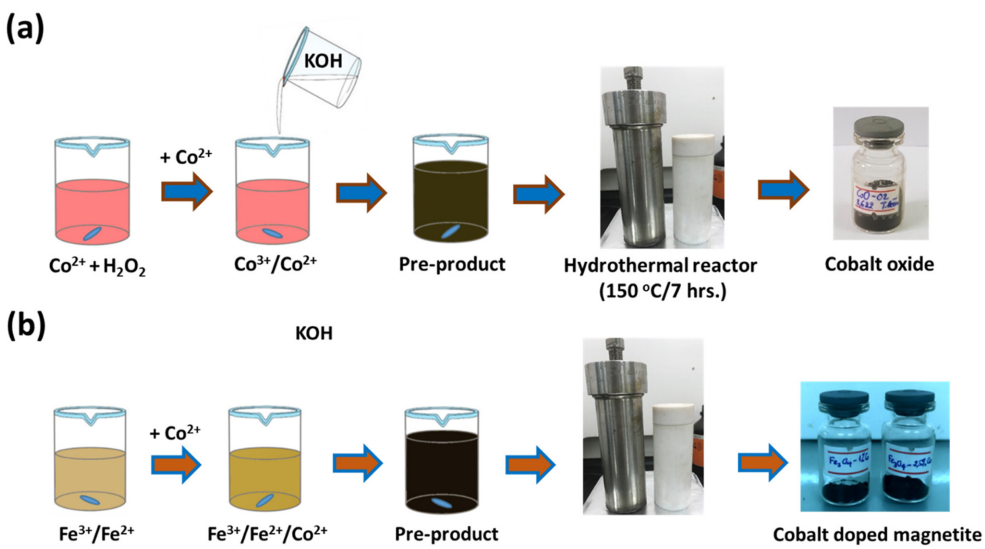

Fig. 1. Schematic representation of hydrothermal synthesis for Co oxide (a) and Co-doped magnetite (b)

(λCuKα = 1.5418 Å, 2θ steps = 0.015°/step).

Field-Emission Scanning Electron Microscope (FE-SEM) observations were made using a Hitachi S-4800.

The average surface charge of the cobalt oxide and Co-doped magnetite nanoparticles was determined using a Zeta Phoremeter IV (CAD Instrumentation) under the applied voltage of 100 Volts at room temperature. Samples were dispersed in distilled water thanks to an ultrasonic bath before being injected into the Zeta cellule. Potassium chloride was used to set the ionic strength. The Schmoluchowski approximation was employed to calculate the Zeta potential values. Each sample was recorded at least 20 times before finally having a good statistic on the diagram distribution and the average surface charge values.

2.3 Electrochemical measurements

Electrochemical impedance spectroscopy (EIS) measurements were performed using three classical electrodes: the working electrode was a rotating cylinder of AA2024, an Ag/AgCl/saturated KCl electrode served as a reference; and a Pt grid as the counter electrode. The EIS measurements were plotted at the frequency range from 100 kHz to 10 mHz at open circuit potential (OCP) with an amplitude of 5 mV. The electrolyte solution was an aqueous solution of 0.05 M NaCl + 0.1 M Na_2SO_4 for the measurement with a naked AA2024 electrode and 0.1 M NaCl for the AA2024 surface covered with epoxy coating. The electrochemical tests were operated with Biologic SP-300 equipment. The measurements were realized at least three time for each sample to ensure the reproducibility of the measurement.

3. Results

3.1 Characterization of synthesized cobalt oxide and cobalt-doped magnetite nanoparticles

Fig. 2 showed XRD patterns for obtained Co oxide and Co-doped magnetite powders.

The XRD patterns of Co-doped magnetite showed that the obtained diffraction peaks at 18.3, 30.1, 35.5, 37.1, 43.0, 53.4, 57.0, and 62.7 degrees coincided with the position of the high crystallinity cobalt ferrite phase, $CoFe_2O_4$ ($Co_xFe_{3-x}O_4$), as previously reported [7], due to the Co^{2+} ion (r = 0.72 Å) efficiently substituted of the Fe^{2+} ion (r = 0.72 Å) in the tetrahedral and octahedral holds in the crystals structure of Fe_3O_4 (reference ICSD # 00-011-0614, cubic crystal structure, *Fd*-3*m*, a ≈ 8.396 Å).

The XRD pattern of synthesized Co oxide nanoparticles shown with principal peaks at 31.6, 37.2, 45.1, 55.9, 59.7, and 65.5 degrees characterize the Co_3O_4 phase (reference ICSD # 01-074-1657, cubic crystal structure, *Fd*-3*m*, a ≈ 8.065 Å). In addition, the other phases, like cobalt oxide hydroxide, CoO(OH) (reference ICSD # 00-007-0169), can be indexed, with principal peaks at 20.4, 39.1, and 50.9 degrees in cobalt oxide samples. The presence of CoO(OH) beside Co_3O_4 phase in the obtained cobalt oxide sample due to the mechanism and transformation process of Co(II)/Co(III) in alkaline media to Co_3O_4 phase does not complete [9].

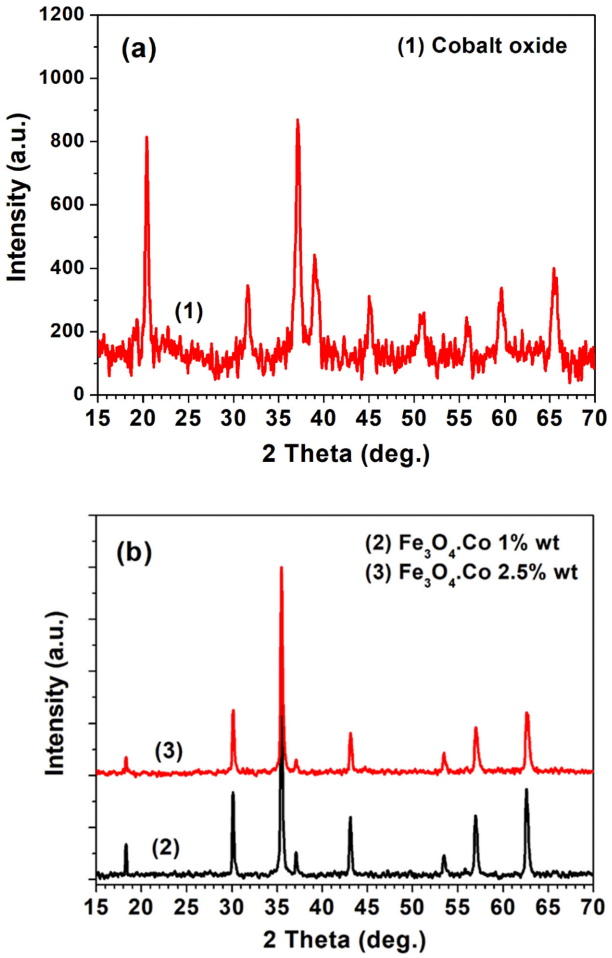

Fig. 2. XRD patterns for Co oxide (a) and Co-doped magnetite (b)

Fig. 3 displays FESEM images for obtained Co oxide and Co-doped magnetite.

It could be seen in Fig. 3 that the morphology of Co oxide particles was relatively homogeneous, with a particle size of about 30 nm. The cube shape for Co-doped magnetite particles was identified [10]. The particle size of Co-doped magnetite for both 1 wt% and 2.5 wt% cobalt content is about 50 nm (Fig. 3b and Fig. 3c). However, some agglomerations were observed for the Co-doped magnetite particles.

The surface charge distribution of the Co oxide and Co-doped magnetite nanoparticles was determined by Zeta potential measurements (Fig. 4). All three diagrams show one main peak, indicating the obtained magnetite Co oxide and Co-doped magnetite particles have a homogeneous surface charge. The

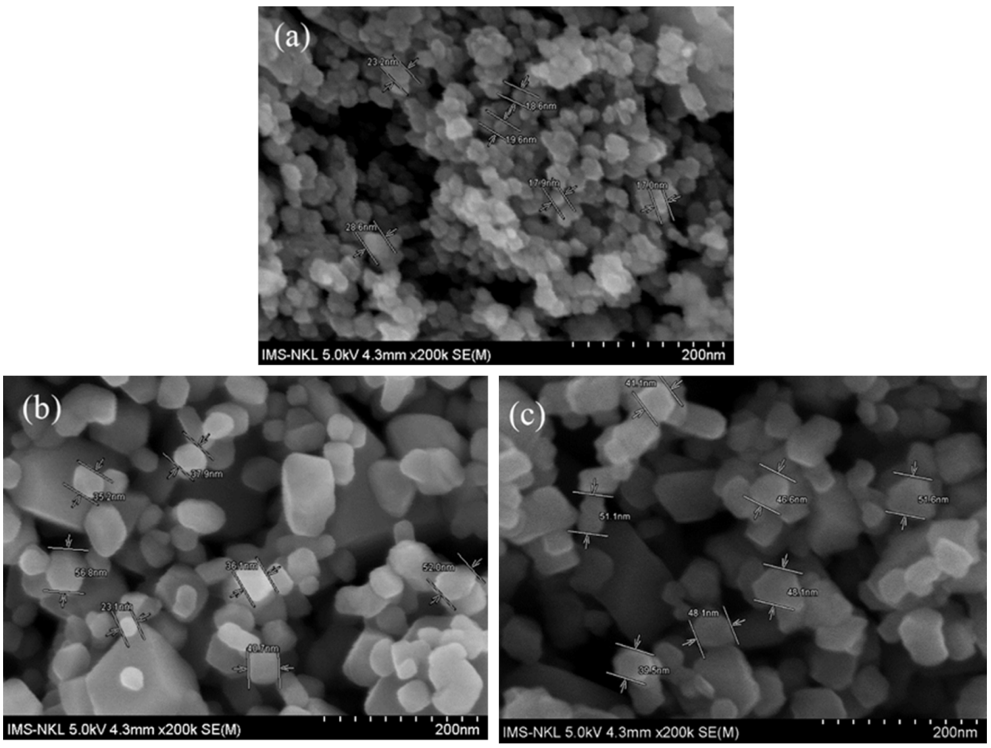

Fig. 3. FE-SEM images of synthesized Co oxide (a) and Co-doped magnetite 1 wt% (b), 2.5 wt% (c)

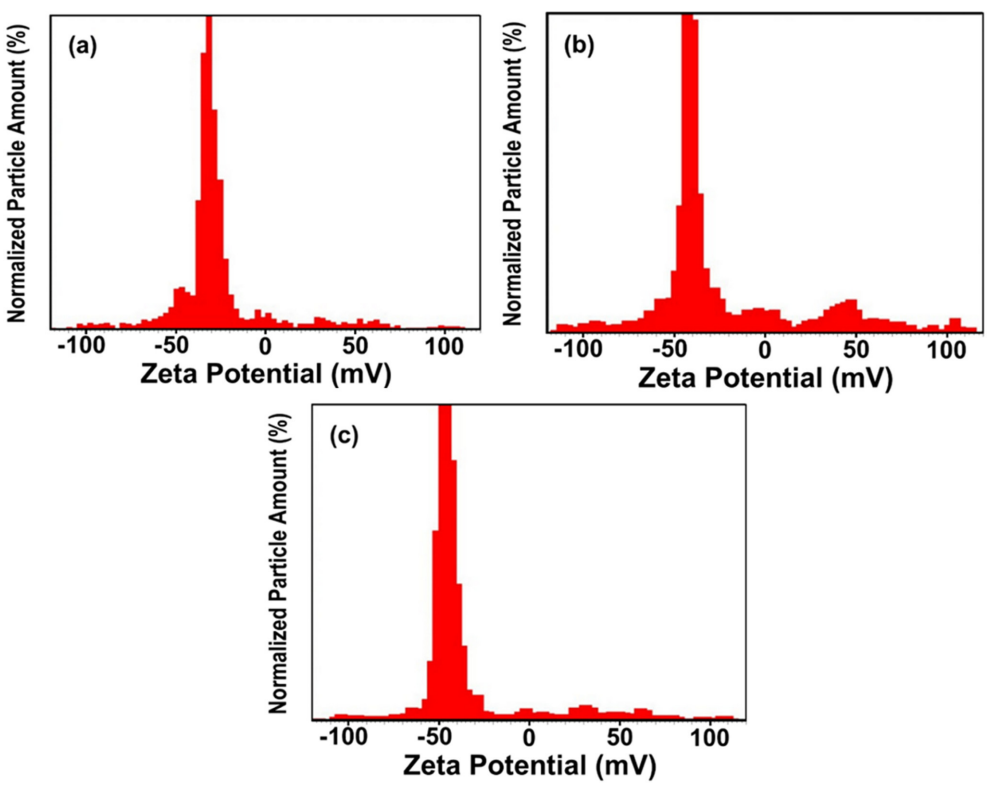

Fig. 4. Surface charge distribution of synthesized Co oxide (a) and Co-doped magnetite 1 wt% (b), 2.5 wt% (c)

average surface charge values were: -25.6 mV, -23.1 mV, and -31.2 mV for the Co oxide, Co-doped at 1 wt%, and 2.5 wt% magnetite, respectively. Herein, the negative charge on the surface of particles resulted from the adsorption/attach of hydroxyl groups (–OH) from the alkaline medium of hydrothermal reaction.

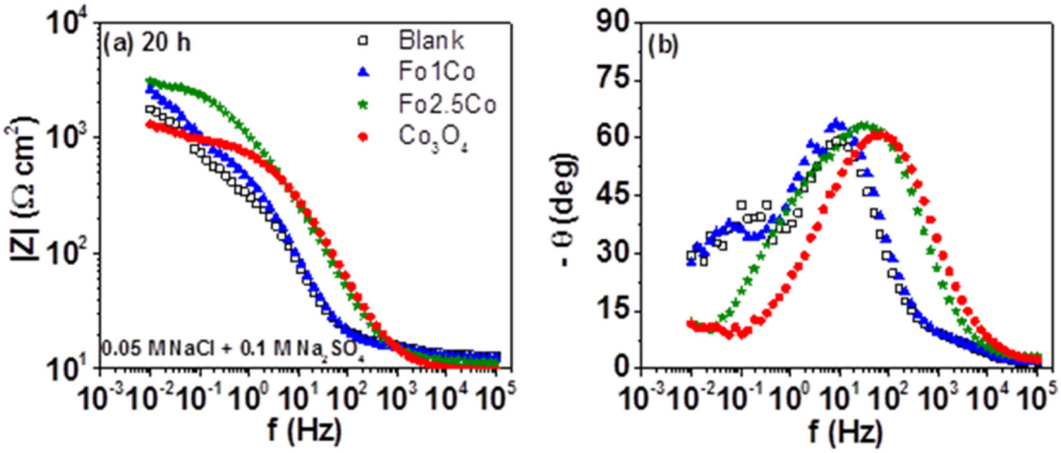

Fig. 5. (a) Bode modulus diagrams and (b) Bode phase angle diagrams of AA2024 electrode after 20 h of immersion in the electrolytic solution containing extract Co oxide and Co-doped magnetite

3.2 Inhibitive property of synthesized Co oxide and Co-doped magnetite nano particles

The corrosion inhibition of Co oxide and Co-doped magnetite nanoparticles was characterized by the electrochemical impedance. Fig. 5 shows EIS Bode diagrams of AA2024 electrode after 20 h exposed in the extracted solution of 1 wt% Co oxide and Co-doped magnetite. A mix of electrolytic salts (0.05 M NaCl + 0.1 M Na_2SO_4) was added to the measured solution. A blank sample, AA2024 electrode immersed in the electrolytic solution, was also measured.

For the blank sample (without nanoparticles), the Bode phase angle diagrams show two-time constants, located at intermediate and low frequency, characterizing the charge transfer on the surface during corrosion processes and the oxygen diffusion. A slight shoulder appeared at the high frequency, attributed to the natural oxide layer existing on the surface [11].

The EIS diagrams for the AA2024 electrode immerging in the extracted solution from Co-doped magnetite with 1 wt% cobalt (Fo1Co) showed the same shape as the reference sample in both modulus and phase angle parts. In this case, non-protection was observed for the electrode immersed in the extract solution of Fo1Co. This could be explained that the presence of Co^{2+} cations in the extract solution was not enough to generate a necessary protection effect.

The EIS diagrams for the AA2024 electrode immerging in the extracted solution of Co oxide and Co-doped magnetite with 2.5 wt% cobalt (Fo2.5Co) gave the same feature, characterized

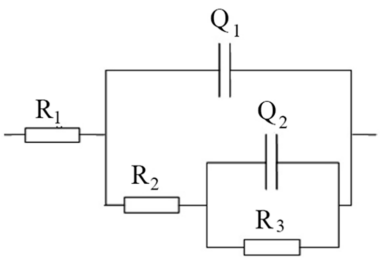

Fig. 6. Equivalent electrical circuit for AA2024 electrode immersed in the extracted solution of Co oxide or Co-doped magnetite

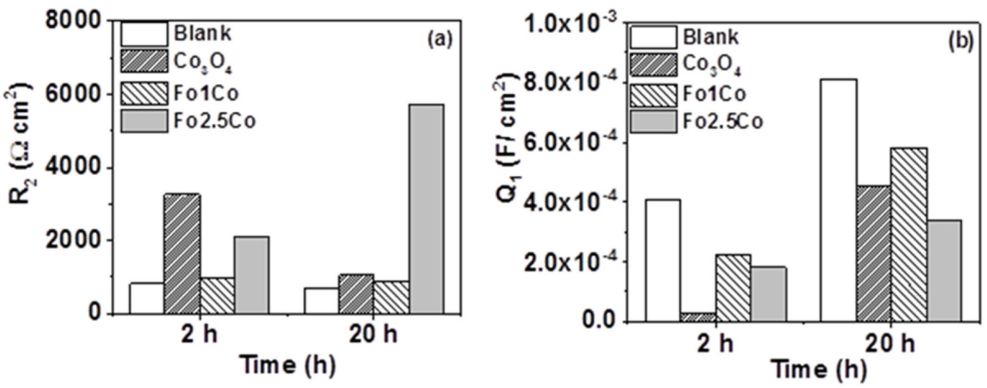

Fig. 7. R_2 (a) and Q_1 (b) values calculated after 2h and 20h immersed in the extract solution of Co oxide and Co-doped magnetite with Co content 1 wt% and 2.5 wt%

by one time constant at high frequency (50 Hz), attributing to the existence of a passive/electrolyte interface film on the AA2024 surface [11]. This film was due to the reaction of the cobalt cations in the extracted solution on the AA2024 surface. The modulus value at the low frequency of the sample with Co oxide was lower than that of Co-doped magnetite Fo2.5Co.

An electrical equivalent circuit (EEC) was used to fit the EIS data (Fig. 6), where R_1: ohmic resistance of the electrolyte, Q_1: constant phase element concerning a capacitance of the oxide layer, R_2: oxide layer resistance, Q_2: constant phase element due to double layer capacitance, and R_3: charge transference resistance. The EIS parameters were calculated from the equivalent circuit and listed in Fig. 7.

It was found in Fig. 7 that the R_2 and Q_1 of the electrode in the Fo1Co solution were compared with the reference sample for a short time (2 hours) and a longer time (20 hours) of the test. This means that at a low concentration of cobalt, the corrosion protection is limited. The highest protection was obtained for the higher concentration of cobalt (2.5 wt%) with a high resistance value and the low CPE value. Fig. 8 provides a schematic of the inhibition reaction of Co^{2+} extract from Co oxide or Co-doped magnetite on the AA2024 surface during immersed in the electrolyte solution. The cathodic reaction occurred on the intermetallic particles of the AA2024 matrix, while Co^{2+} cations released from Co oxide and Co-doped magnetite particles could be precipitated in the form of hydroxide film according to equations:

$$2H_2O + O_2 + 4e \rightarrow 4OH^- \quad (1)$$

$$Co^{2+} + 2OH^- \rightarrow Co(OH)_2\downarrow \quad (2)$$

Therefore, the precipitate layer could cover and limit the cathodic activity of the intermetallic particles; the oxide/hydroxide film on the AA2024 surface consisted of Al_2O_3/$Al(OH)_3$ + $Co(OH)_2$ mixture. This hypothesis is similar to the AA2024 electrode in the electrolyte containing Co^{2+} cations in the previous work [12].

3.3 Characterization of protective property of epoxy coating containing Co oxide and Co-doped magnetite nano particles

The corrosion protection of an epoxy resin containing Co oxide and Co-doped magnetite nanoparticles was evaluated by EIS measurements during immersion in the 0.1 M NaCl solution. The concentration of nanoparticles in the coating was fixed at 5 wt%, at higher content of nanoparticles; the protective property was not improved, as mentioned in the document [13]. In addition, the Co-doped magnetite with 2.5 wt% of cobalt content was incorporated in the epoxy resin; at lower content of cobalt doped (1 wt%); it did not show any effect for corrosion protection, as presented in Figs. 5 and 7.

Fig. 9 displays as an example the Bode diagrams of the AA2024 plate covered by epoxy coating (reference) and an epoxy coating containing 5 wt% of Co-doped magnetite nanoparticles during immersion time in the electrolytic solution (0.1 M NaCl).

For the reference sample, from the first day of the test, the EIS diagrams presented two well-defined time constants, the first located at high frequency characterizing the coating and the second in the low-frequency range attributed to the oxide

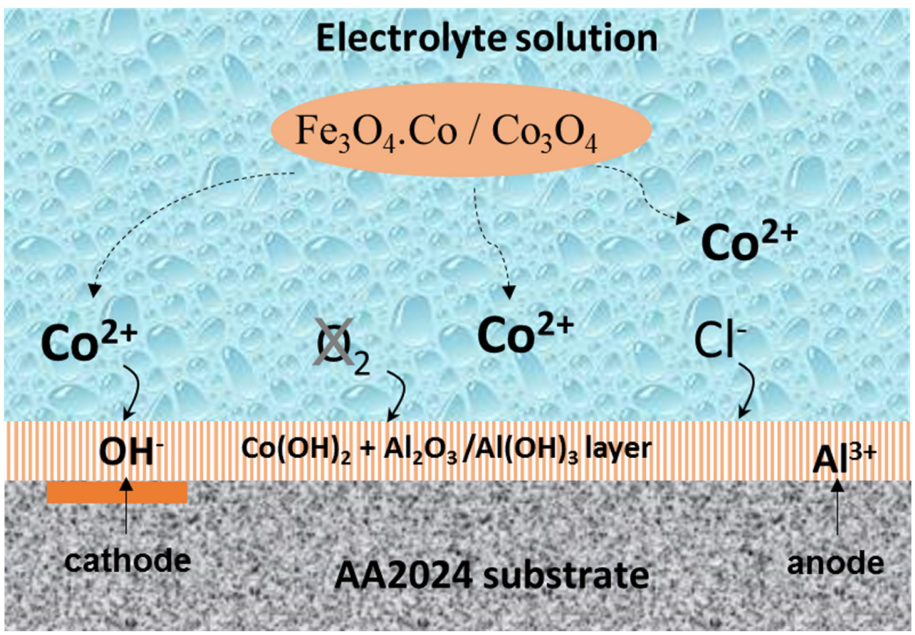

Fig. 8. Schematic representation of the inhibition reaction by Co oxide and Co-doped magnetite particles extract on the AA2024 surface during immersed in the electrolyte solution

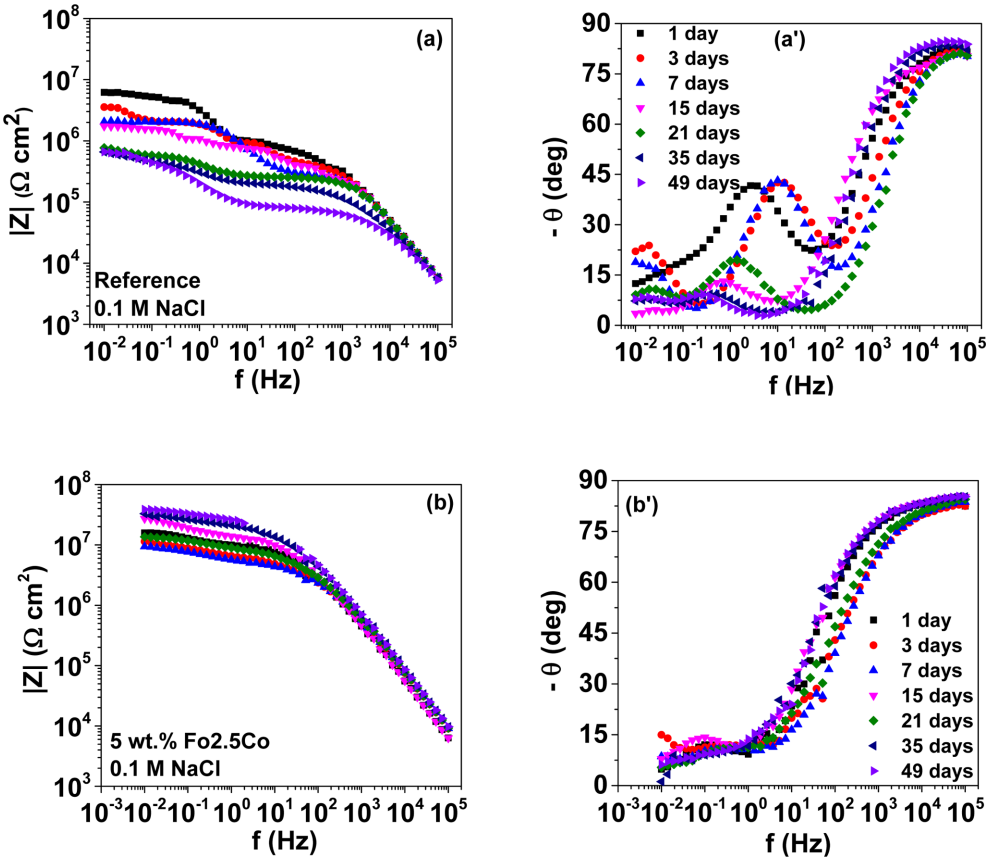

Fig. 9. Bode diagrams of AA2024 surface covered by epoxy coating (a, a') and epoxy coating containing 5 wt% of Co-doped magnetite nano particles with Co content of 2.5 wt% (b, b')

layer on the AA2024 surface. Correspondingly, the values of modulus (Fig. 7a) continuously decreased during exposing time. This evolution of EIS diagrams indicated a quick degradation process of the epoxy coating.

In the presence of Co-doped nanoparticles, the shape of EIS spectra remained identically during immersion time in the electrolytic solution (Fig. 9b and 9b'). The phase angles illustrate only one time constant at high frequency; and there was a slight variation in the modulus values with immersion time. This EIS shape characterizes a good barrier effect of the coating; in this case, the coating/AA2024 interface reaction was limited, and the low-frequency behavior is not well defined. In addition, the stabilizing of EIS diagrams during a long time of measurement (49 days) demonstrates high protection of the epoxy coating containing Co-doped nanoparticles.

It is a remark that phase angle at 10 kHz for loaded coating remained constant while blank sample shows decreasing behavior of phase angle with immersion time. It is attributed to the high resistive property of the epoxy coating loaded with Co oxide and Co-doped magnetite compared with blank coating. It was possible that the pigment particles interacted with the epoxy resin during the hardening of the polymer due to the high polarity of Co oxide and Co-doped magnetite. These interactions

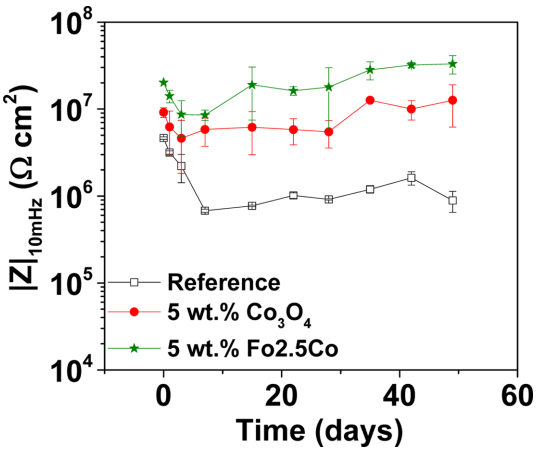

Fig. 10. $|Z|_{10mHz}$ values versus immersion time in the 0.1 M NaCl solution

led to an improvement of the crosslink in the coating and hence might be responsible for a decrease in the diffusion of water molecules and ions into the film.

According to the literature, the corrosion inhibition of the coating could be monitored by the variation of modulus values at a low frequency during exposing time [14]. In Fig. 10, the

modulus values at 10 mHz ($|Z|_{10mHz}$) for the reference sample continuously fell in 7 days and remained constantly at a low value of ($|Z|_{10mHz}$) till the end of the test.

For the coating containing Co oxide, $|Z|_{10mHz}$ values rapidly decreased in 3 days; after that, this parameter rested stably at the value of 10 times higher compared with reference coating. A similar tendency was observed for the coating containing Co-doped magnetite particles, but these $|Z|_{10mHz}$ values were higher than the sample containing Co oxide.

The decrease of $|Z|_{10mHz}$ values at the initial time was due to the penetration of the water and electrolytes through the epoxy coating; hence the film resistance values decreased with the immersion time. The dispersion of nano oxide in the epoxy resin generated tortuous ways inside the coating and consequently prolonged the transport of the water and electrolyte in the coating; therefore; the barrier effect was improved, as shown in Fig. 9b.

It was shown in Fig.s 7 and 8 that the Co^{2+} cations could release from Fe_3O_4.Co and Co_3O_4 particles inhibit the corrosion reaction of AA2024 surface by forming cobalt hydroxide at cathodic sites where the OH^- anions were produced. This process is accompanied by the penetration of water and electrolytes in the coating; therefore, the Co^{2+} lixiviation could create new microchannels in the epoxy coating. After 3 days of immersion for the coating loading Co oxide and 7 days for the coating loading Co-doped magnetite, a ascend–descend trend of $|Z|_{10mHz}$ values was evident. This might be due to the interface action of Co^{2+} cations at the coating/AA2024 interface, which could form an interfacial film but also penetrate to seal the micropores of the coating; hence the protective effect was improved, the modulus values could re-increase as presented in Fig. 10. The interface reaction in the presence of Co^{2+} cations might also promote the coating adhesion at the AA2024 surface; hence until a long time (49 days) of the test, the low-frequency behavior in Fig. 9b was not well defined.

4. Conclusions

Cobalt oxide and cobalt-doped magnetite nanoparticles were synthesized via the hydrothermal method. The corrosion inhibition of the synthesized products depends on the cobalt content; at low content (1 wt% of cobalt in the Co-doped magnetite), the inhibitive effect was limited. The Co oxide and Co-doped magnetite (2.5 wt% of Co content) were incorporated into the water-based epoxy coating. The EIS results revealed that the presence of both Co oxide and Co-doped magnetite significantly improved the protection property of the epoxy coating. This enhancement is attributed to forming a cobalt hydroxide film beneath the epoxy coating. The Co-doped magnetite nanoparticle gave more efficiency than Co oxide for corrosion protection of aluminum 2024 surface.

Acknowledgements

The authors would like to thank VAST for the funding support under project NCVCC13.06/20-20.

References

1. Henry Leidheiser Jr., and Ichiro Suzuki, Cobalt and Nickel Cations as Corrosion Inhibitors for Galvanized Steel, *Journal of The Electrochemical Society*, **128**, 242 (1981). Doi: https://doi.org/10.1149/1.2127399
2. Henry Leidheiser, Jr. and Gary W. Simmons, Mössbauer Spectroscopic Study of the Corrosion Inhibition of Zinc by Coigesalt Ions, *Journal of The Electrochemical Society*, **129**, 1658 (1982). Doi: https://doi.org/10.1149/1.2124231
3. M. A. Jakab, F. Presuel-Moreno and J. R. Scully, Effect of Molybdate, Cerium, and Cobalt Ions on the Oxygen Reduction Reaction on AA2024-T3 and Selected Intermetallics, *Journal of The Electrochemical Society*, **153**, B244 (2006). Doi: https://doi.org/10.1149/1.2200300
4. M. Rostami, S. Rasouli, B. Ramezanzadeh, A. Askar, Electrochemical investigation of the properties of Co doped ZnO nanoparticle as a corrosion inhibitive pigment for modifying corrosion resistance of the epoxy coating, *Corrosion Science*, **88**, 387 (2014). Doi: https://doi.org/10.1016/j.corsci.2014.07.056
5. E. Ghasemi, B. Ramezanzadeh, S. Saket, S. Ashhari, Electrochemical investigation of the epoxy nanocomposites containing $MnAl_2O_4$ and $CoAl_2O_4$ nanopigments applied on the aluminum alloy 1050, *Journal of Coatings Technology and Research*, **13**, 97 (2016). Doi: https://doi.org/10.1007/s11998-015-9728-6
6. J. A. Sturgill, A. W. Phelps, J. T. Swartzbaugh, Nontoxic corrosion protection pigments based on cobalt, US Patent No 7833331 B2, 16 November (2010). https://patents.google.com/patent/US7833331B2/en
7. Trinh Anh Truc, Nguyen Xuan Hoan, Dang The Bach, Thai Thu Thuy, Kavitha Ramadass, C. I. Sathish, Nguyen Thuy Chinh, Nguyen Duy Trinh, and Thai Hoang, Hydrothermal Synthesis of Cobalt Doped Magnetite Nanoparticles for Corrosion Protection of Epoxy Coated Reinforced Steel, *Journal of Nanoscience and Nanotechnology*, **20**, 3519 (2020). Doi: https://doi.org/10.1166/jnn.2020.17413
8. Le Quoc Long, Tran Thi Bich Hue, Nguyen Xuan Hoan, Le Viet Cuong, Pham Duc Thang, Thai Hoang and Trinh Anh Truc, Growth Mechanism and Stability of Magnetite

Nanoparticles Synthesized by the Hydrothermal Method, *Journal of Nanoscience and Nanotechnology*, **16**, 7373 (2016). Doi: https://doi.org/10.1166/jnn.2016.11110

9. Zhifang Huang, Yan Zhao, Yuehong Song, Yawen Li, Gongjuan Wu, Hongjiao Tang and Jingzhe Zhao, Study on the oxidation process of cobalt hydroxide to cobalt oxides at low temperatures, *RSC Advances*, **6**, 80059 (2016). Doi: https://doi.org/10.1039/C6RA16063H
10. T. Ishikawa, H. Nakazaki, A. Yasukawa, K. Kandori, and M. Seto, Infuences of Co^{2+}, Cu^{2+}, and Cr^{2+}, ions on the formation of magnetite, *Corrosion Science*, **41**, 1665 (1999). Doi: https://doi.org/10.1016/S0010-938X(98)00198-X
11. G. Boisier, thèse de doctorat, Université de Toulouse, 93 (2018).
12. Thu Thuy Thai, Anh Truc Trinh, Gia Vu Pham, Thi Thanh Tam Pham, Hoan Nguyen Xuan, Corrosion Protection Properties of Cobalt Salt for Water-Based Epoxy Coatings on 2024-T3 Aluminum Alloy, *Corrosion Science and Technology*, **19**, 8 (2020). Doi: https://doi.org/10.14773/cst.2020.19.1.8
13. T. X. H. To, A. T. Trinh, H. N. Truong, K. O. Vu, J-B Jorcin, N. Pébère, Corrosion protection of carbon steel by an epoxy resin containing organically modified clay, *Surface & Coatings Technology*, **201**, 7408 (2007). Doi: https://doi.org/10.1016/j.surfcoat.2007.02.009
14. T. T. Thai, M.-E. Druart, Y. Paint, A. T. Trinh, M.-G. Olivier, Influence of the sol-gel mesoporosity on the corrosion protection given by an epoxy primer applied on aluminum alloy 2024 –T3, *Progress in Organic Coatings*, **121**, 53 (2018). Doi: https://doi.org/10.1016/j.porgcoat.2018.04.013